Seismic Performance Assessment Of Inadequately Detailed Reinforced Concrete Columns

A. Boys, D. K. Bull and S. Pampanin

University of Canterbury, Christchurch, New Zealand

2008 NZSEE Conference

ABSTRACT: Existing New Zealand building stock contains a significant number of structures designed prior to 1995 with inadequate detailing of the internal or 'gravity' reinforced concrete (RC) columns. Typically these columns have insufficient transverse reinforcement; lap-splices in the plastic hinge region; and longitudinal bars that are 'cranked' at the end of the lap-splice. Columns with such details have been shown to perform poorly when subjected to seismic demand, losing axial load carrying capacity at drift levels less than the building is expected to be subjected to during a design level earthquake.

This paper outlines an investigative program to determine the susceptibility of these gravity columns to axial collapse. A drift based backbone capacity model for shear and subsequent axial failure is presented which has been verified by experimental testing performed to date. Such experimental tests have highlighted the susceptibility of these inadequately detailed columns to lose axial load capacity at drift levels significantly below the seismic demand on such structures due to a design level earthquake.

1 INTRODUCTION

1.1 Background

Existing New Zealand building stock contains a significant number of structures designed prior to the revision of NZS 3101 in 19995 with inadequate detailing of the internal or 'gravity' reinforced concrete (RC) columns. While the requirements for shear, anti-buckling and confinement lead to adequate transverse reinforcement detailing of the moment resisting frame (MRF) columns in NZS3101 1982, the internal columns did not have matching requirements. This is a considerable oversight as the columns while not specifically considered to contribute to the lateral force resisting mechanism still undergo the same displacement demands as the MRF columns. As illustrated by previous earthquakes (see Figure 1a) and b)) these columns are subject to damage associated with the displacement history of the structure, and as such potentially lose axial capacity, leading to incipient collapse of the structure.

Previous studies in the United States have investigated the axial failure of similarly detailed columns (Lynn et al. 1996) and (Melek et al. 2003). Lynn et al tested eight columns (with a range of reinforcement details) uni-directionally in double curvature. These tests highlighted the susceptibility of inadequately detailed columns to lose axial capacity at moderate levels of drift (~2-3%). Melek et al tested six cantilever columns with lap-splices uni-directionally under a range of axial loads. Further investigation is necessary particularly regarding the effect of bi-directional bending on the degradation of the columns and the associated loss of axial carrying capacity.

A significant departure from previous work in this area that pertains to existing New Zealand building stock is the practice of cranking the longitudinal bars at the top of the lap-splice. The cranked bars are susceptible to buckling which may initiate shear failure and the associated loss of axial capacity.

a) Parking Building, California State University, Northridge, 1994

b) Indian Hills Medical Centre, Northridge, 1994

Figure 1: Previous Inadequately Detailed Column Failures

1.2 **Shear Failure and Loss of Axial Load Capacity**

The most significant failure mechanism inherent in the inadequately detailed gravity columns is the loss of axial load carrying capacity. Elwood and Moehle (2006) recently proposed an idealised backbone model for the capacity of these columns. The model developed is empirical in nature and as such is applicable only to columns with appropriate details and test configuration(Elwood and Moehle 2005a). Figure 2 a) below illustrates the backbone capacity model developed compared with results from an experimental test. The model has a shear capacity equal to the plastic capacity of the column (as determined by moment-curvature analysis). Detailing dependent drift levels are calculated for the yielding of the section, shear failure (indicated by a reduction of capacity to below 80% of maximum); and post shear-failure loss of axial load carrying capacity.

For the purposes of the paper only relationships for shear and axial failure will be illustrated. The drift capacity at shear failure can be found from (Elwood and Moehle 2005a):

$$\delta_s = \frac{3}{100} + 4\rho'' - \frac{1}{40}\frac{\upsilon}{\sqrt{f'_c}} - \frac{1}{40}\frac{P}{A_g f'_c} \geq \frac{1}{100} \qquad \textbf{1}$$

where ρ" = transverse steel volumetric ratio, υ = nominal shear stress, f'_c = concrete compressive strength, P = the axial load on the column, and A_g = gross cross-sectional area.

Axial failure of the columns is dependent on prior shear failure and force equilibrium at the shear failure plane (see Figure 2 b)). Force equilibrium is used in conjunction with experimental data to derive the following relationship for drift at axial failure (Elwood and Moehle 2005b):

$$\delta_a = \frac{4}{100}\frac{1+\tan^2 65°}{\tan 65° + P\left(\dfrac{s}{A_{st} f_{yt} d_c \tan 65°}\right)} \qquad \textbf{2}$$

where 65° is the assumed angle of the shear failure plane, A_{st} = area of transverse reinforcement parallel to the applied shear and having spacing s, f_{yt} = yield stress of transverse reinforcement, and d_c = depth of column core measure parallel to the applied shear.

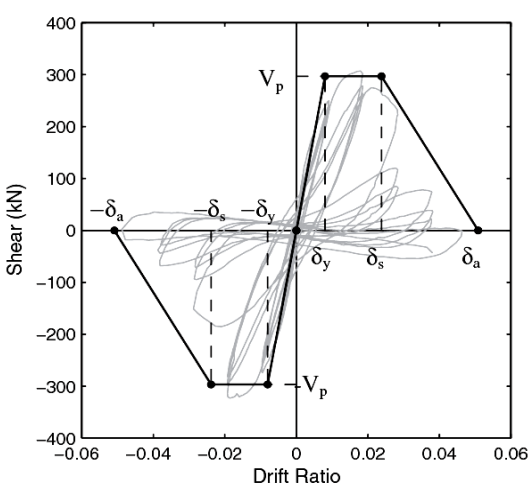

a) Idealised Backbone

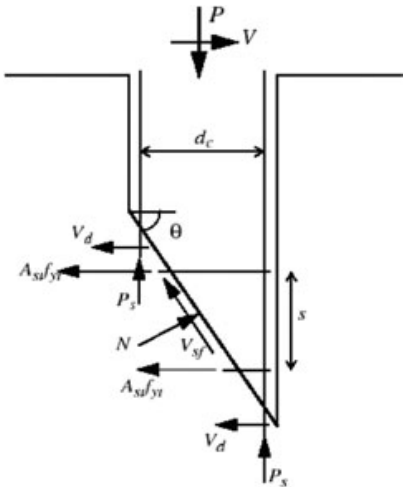

b) Free Body Diagram of Shear Failure Plane

Figure 2: Idealised Backbone Model and Shear Failure Plane (Elwood and Moehle 2006)

2 EXPERIMENTAL PROGRAM

2.1 Specimen Selection

Design of the test columns was undertaken with consideration regarding the limitations imposed by the proposed models, the test apparatus, and consultation with practising professional engineers to ensure realistic detailing. The specimens are 450mm square cantilever columns with a height (to the application of lateral load) of 1624 mm; Figure 3 a) illustrates an elevation of a typical column. All specimens have four D25 Grade 300 reinforcing bars (longitudinal reinforcing ratio = 1%), R10 stirrups at 300mm spacing (minimum diameter and maximum spacing allowable, transverse reinforcing ratio = 0.12%), and cranked bars at the end of the lap-splice (see Figure 3 b)). A concrete compressive strength (f'_c) of 32 MPa was targeted to reflect nominal design strength of 24 MPa with a 33% increase in long-term in-situ strength. Two lap-splice lengths are chosen; 600mm corresponding to the minimum allowable (24 d_b) and 750mm (30 d_b) to reflect a more conservative design.

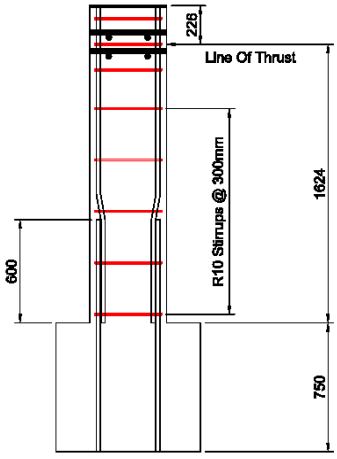

a) Specimen Elevation

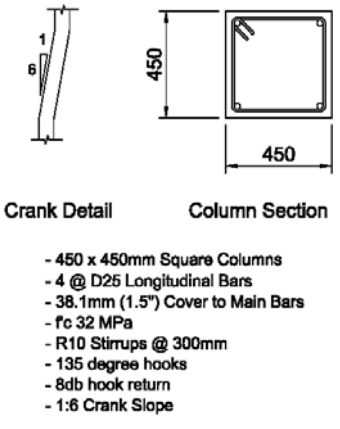

b) General Section Details

Figure 3: Specimen Details

An experimental program of six tests is proposed, which is outlined in Table 1. The first four tests comprise specimens with 600mm and 750mm lap-splice length, loaded under 2D and 3D quasi-static displacement histories. An axial load of 2000kN was chosen as the likely upper limit of gravity columns in existing buildings. The specimen in test five is a 600mm lap-splice specimen, subjected to reduced axial load (1000kN) and bi-directional lateral loading. The purpose of this test is to extend the verification of the models presented to a structure with a more moderate level of axial load. The specimen in test six is a 600mm lap-splice specimen, loaded under a quasi-earthquake displacement protocol. The aim of this test is to verify that the quasi-static loading protocol is excessively demanding and illustrate that under a more realistic seismic demand the specimen will have increased displacement capacity.

Table 1 Proposed Experimental Program

Specimen Designation	Lap length	Tie Details	Axial Load	Loading Protocol
24L-300-2D	600mm (24 d_b)	R10 @ 300mm	2000kN (0.3f'$_c$A$_g$)	2D Quasi-Static
24L-300-3D	600mm (24 d_b)	R10 @ 300mm	2000kN (0.3f'$_c$A$_g$)	3D Quasi-Static
30L-300-2D	750mm (30 d_b)	R10 @ 300mm	2000kN (0.3f'$_c$A$_g$)	2D Quasi-Static
30L-300-3D	750mm (30 d_b)	R10 @ 300mm	2000kN (0.3f'$_c$A$_g$)	3D Quasi-Static
24L-300-3D-R	600mm (24 d_b)	R10 @ 300mm	1000kN (0.15f'$_c$A$_g$)	3D Quasi-Static
24L-300-EQ	600mm (24 d_b)	R10 @ 300mm	2000kN (0.3f'$_c$A$_g$)	3D Quasi-EQ

2.2 **Loading Protocols**

As illustrated in Figure 4 a) the 2D displacement protocol comprises three cycles at the following levels of drift; 0.1%, 0.25%, 0.5%, 0.75%, 1.0%, 1.5%, 2.0%, 3.0%, 5.0% (Melek et al. 2003). While it is generally considered that 3 cycles at each drift level is excessive when testing sub-assembly components corresponding to existing structures, this protocol was selected to coincide with previous tests to enable comparisons. Figure 4 b) illustrates that the 3D displacement protocol comprises one cycle of a clover leaf pattern in addition to one cycle in both directions (X and Y) in uni-directional bending only. Scaling of the clover-leaf is such that the maximum drift in both the X and Y directions for each cycle is identical to the 2D protocol. This is to ensure that the specimen undergoes three peaks to each drift level in both directions as illustrated in Figure 5 a) and b), allowing the effects of bi-directional loading to be assessed without additional loading cycles applied to the specimen.

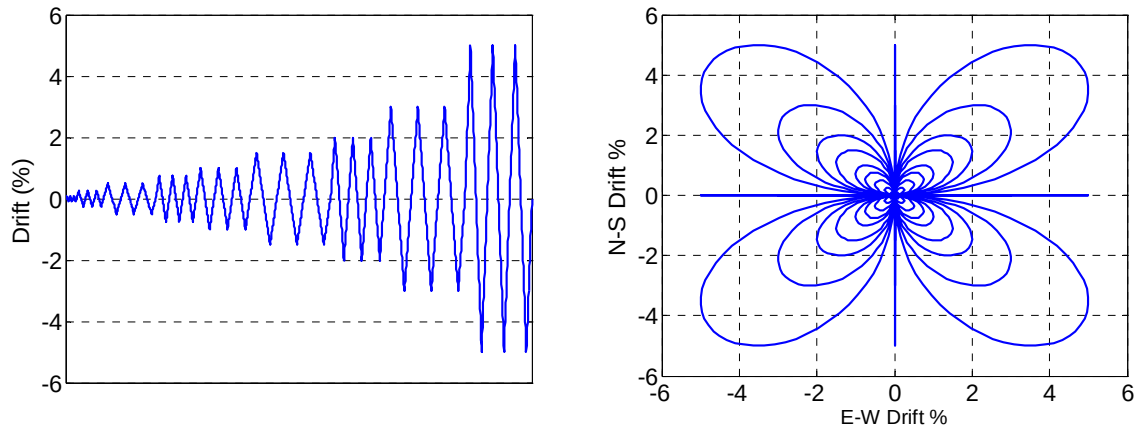

a)2D Drift Protocol **b)3D Drift Protocol**

Figure 4: 2D and 3D Displacement Protocols

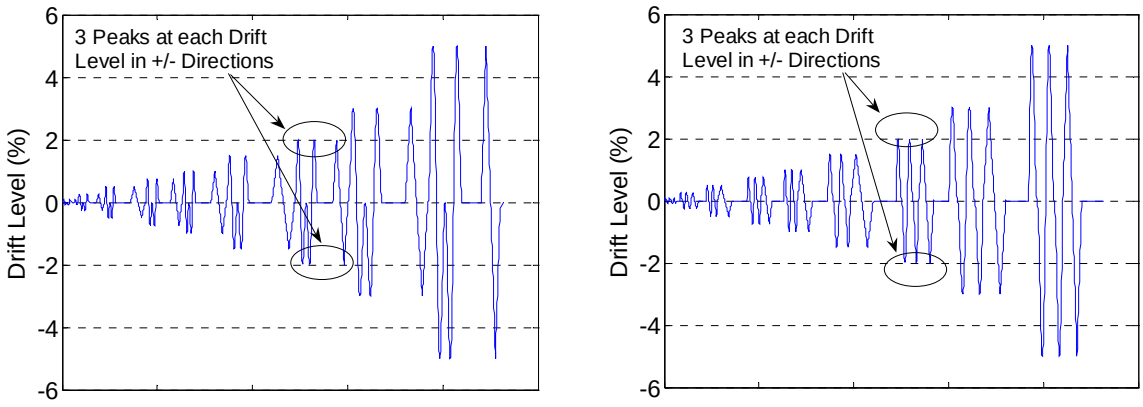

a) N-S Component of 3D Drift Protocol **b) E-W Component of 3D Drift Protocol**

Figure 5: Components of the 3D Displacement Protocol

2.3 Test Apparatus

The test apparatus allows the cantilever columns to be loaded axially in addition to bi-axial bending. Figure 6 a) illustrates the schematic of the lateral force application via a self-equilibrating frame and counterweight to ensure lateral force application is via the hydraulic rams alone. Pivots are located at the top and base of the column allowing the reaction frame to rotate at the base and induce bending in the column. Axial load is applied using the Dartec, which has an adjustable reaction head and a ram extending from the floor. The experimental set-up for bi-directional bending is shown in Figure 6 b).

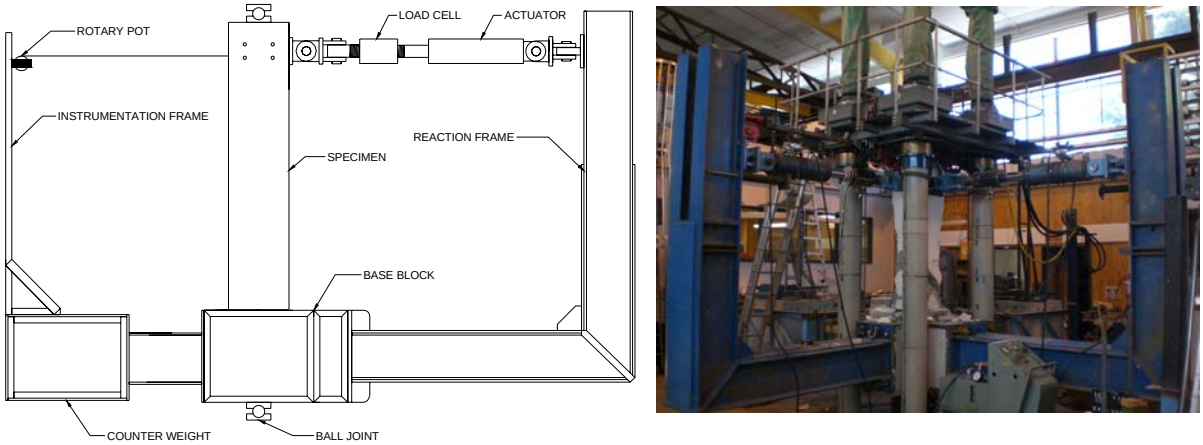

a) Elevation of Test Apparatus **b) Test Apparatus**

Figure 6: Diagram and Photograph of Test Apparatus

3 EXPERIMENTAL RESULTS AND MODEL COMPARISONS

3.1 Experimental Program Status

Two tests of the program have been completed to date; specimen 24L-300-2D (600 mm lap-splice, tested under the 2D quasi-static loading protocol), and specimen 24L-300-3D (600 mm lap-splice, 3D protocol). Both tests were accompanied by material tests to enable accurate calculation of the models.

3.2 **Material Properties**

Table 2 Material Properties

Column Designation	f'_c (MPa)	f_y (MPa)	f_u (MPa)	f_{yt} (MPa)
24L-300-2D	33.6	315	465	439
24L-300-3D	28.4	315	465	439

3.3 **24L-300-2D Specimen Test**

The progression of damage exhibited by the 24L-300-2D specimen as it proceeds to failure on the first reverse cycle to -3.0% drift is shown below in Figure 7 a) - f). Flexural cracks appear in the cycles at 1.0% drift, shear cracks appear in the cycles at 1.5% drift and splice-plane failure is developed during the cycles at 2.0% drift. Lateral capacity starts to degrade significantly after the splice shearing expels the corner cover, allowing the shear failure plane to fully develop. Shear failure occurs on the first excursion to +3.0% and the subsequent axial failure occurring on the reverse cycle to -3.0% drift. The axial deformation was limited during the test to a maximum of 25mm to ensure the safety of the personnel and to reduce the risk of damaging the test apparatus. At the final position data was recorded at the axial load applied to the column was 433kN.

After completion of the test and removal from the test apparatus the loose damaged concrete was cleared to allow an unobstructed view of the failure mechanisms of the column. In Figure 7 g) the shear failure plane is clearly evident in addition to the buckling of the cranked bars as the column deformed axially. As the column deformed axially there was a corresponding increase in lateral expansion causing the stirrup crossing the shear failure plane to burst one of the 135 degree hooks off the longitudinal bar it was restraining.

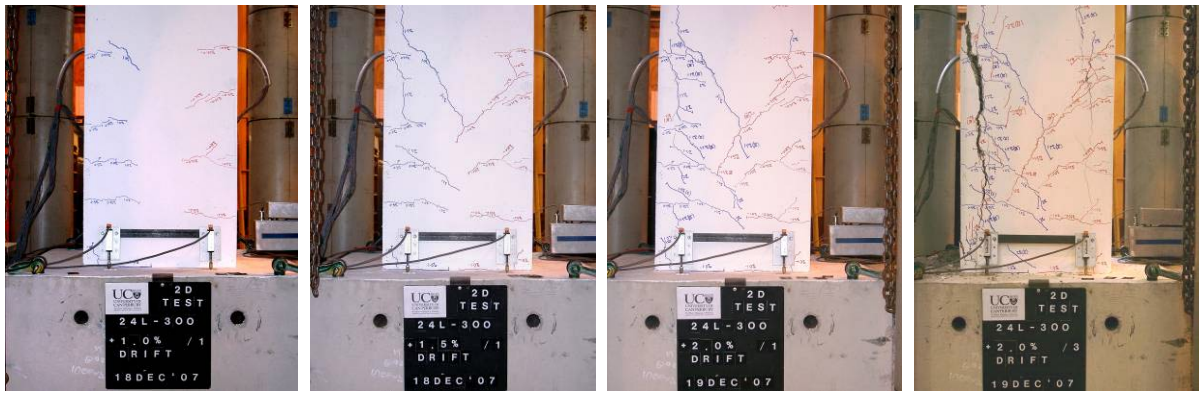

a) 1.0% Drift **b) 1.5% Drift** **c) 2.0% Drift – 1st Cycle** **d) 2.0% Drift – 3rd Cycle**

e) +3.0% Drift **f) -3.0% Drift (Axial Failure)** **g) Buckling of Cranked Bars** **h) Burst Stirrup at Hook**

Figure 7: Progression of Damage for Test Specimen 24L-300-2D

The backbone model for the 24L-300-2D specimen is shown below in Figure 8 a). Included in the figure are: section force-displacement capacity; shear failure limit; and the drift at loss of axial capacity. From the model shear failure is calculated to occur at a drift of 35.5 mm where the section capacity and the shear failure limit intersect. In the model as axial failure is assumed to follow the shear failure. However Figure 8 a) illustrates the calculated drift at axial failure occurs prior to the shear failure drift limit, and therefore the drift limit for axial failure is increased to match the drift at shear failure.

Figure 8 b) compares the backbone model with the experimental data for the test specimen. It is evident that the model captures the behaviour adequately with shear failure occurring on the first cycle to +3.0% drift just prior to the modelled drift limit. Although the column exceeds the shear drift limit the capacity is significantly reduced below the 80% of maximum at which shear failure is deemed to occur. While the loss of axial capacity did not occur immediately following the shear failure it occurred after minimal additional demand.

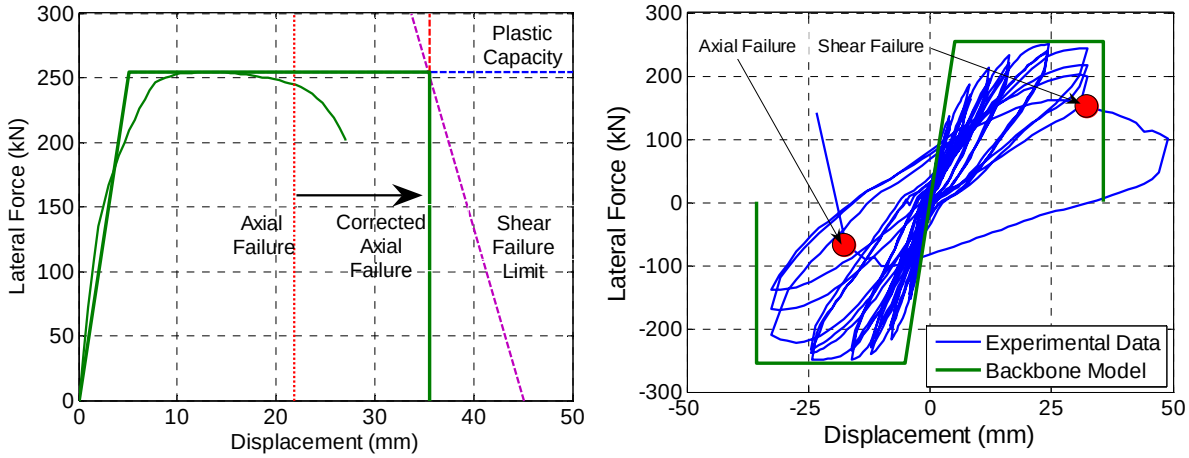

a) Backbone model

b) Experimental Comparison

Figure 8 Backbone Model and Experimental Comparison for Specimen 24L-300-2D

3.4 **24L-300-3D Specimen Test**

The progression of damage exhibited by the 24L-300-3D specimen as it proceeds to axial failure on the second 'leaf' of the loading protocol at 1.5% drift is shown below in Figure 9 a) - f). Flexural cracks appear in the cycles at 0.5% drift, shear cracks appear in the cycles at 0.75% drift and splice-plane failure is developed during the cycles at 1.0% drift. Shear failure occurs on the first 'leaf' of the loading protocol at 1.5% and the subsequent axial failure occurring on the subsequent 'leaf'. Figure 10 a) illustrates the point in the loading protocol at which the shear and axial failures occurred. The residual axial capacity of the specimen when the test was ended at an axial displacement of 25 mm was not recorded by the data acquisition system.

After completion of the test and removal from the test apparatus the loose damaged concrete was cleared to allow an unobstructed view of the failure mechanisms of the column. In Figure 9 g) the buckling of the cranked bars is evident and in Figure 9 h) the shear failure cone is shown.

Figure 10b) develops the backbone model for the test specimen. Both the shear limit and the drift capacity at axial failure were calculated for a 45 degree applied force (resolved to component at zero degrees). Forty-five degrees corresponds to the minimum effectiveness of the transverse reinforcement to restrain the shear failure plane. The shear failure drift (and the corrected drift at axial failure) are found at the intersection of the backbone capacity for a lateral force applied at zero degrees, as this corresponds to the maximum uni-axial displacement. In addition Figure 10 b) illustrates section

capacity (resolved into the component at zero degrees) for a lateral force applied at 30 degrees (the maximum displacement in each 'leaf' occurs at a 30 degree angle to the corresponding axes). Resolving the capacities and limits into components allows direct performance comparisons between uni- and bi-direction demands.

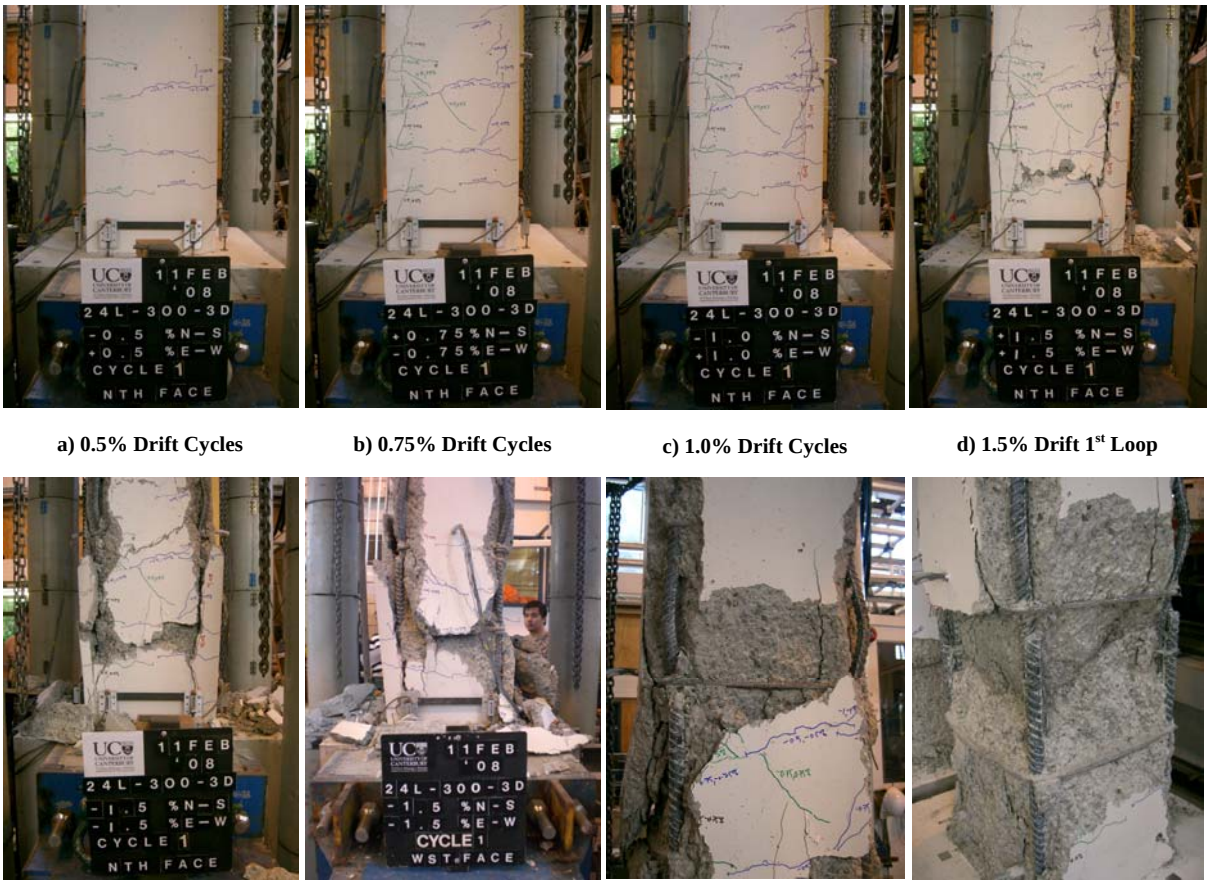

a) 0.5% Drift Cycles **b) 0.75% Drift Cycles** **c) 1.0% Drift Cycles** **d) 1.5% Drift 1st Loop**

e) Failure (North Face) **f) Failure (West Face)** **g) Buckled Cranked Bars** **h) Shear Failure Cone**

Figure 9 Progression of Damage for 3D Specimen

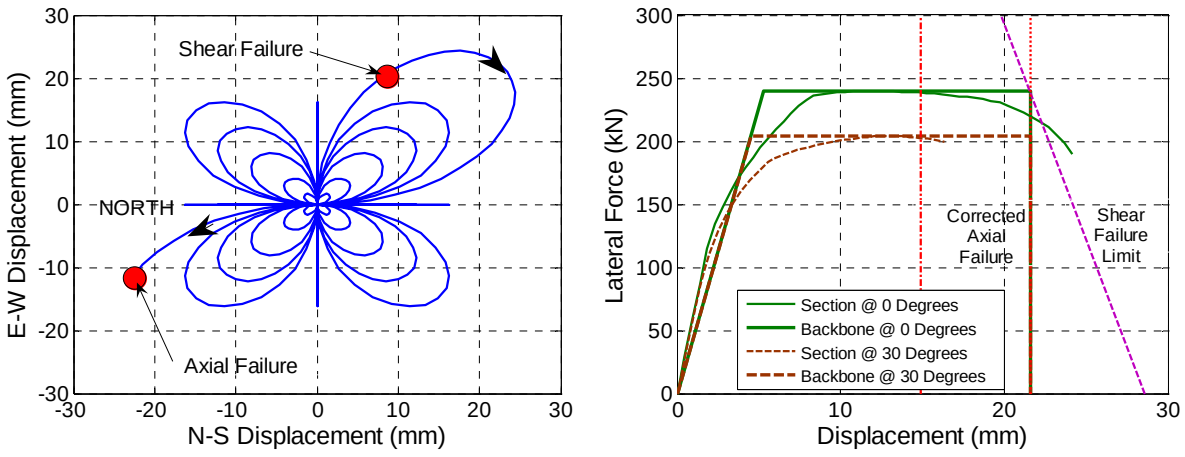

a) Path to Failure **b) Backbone Model**

Figure 10: Loading Path to Failure and Backbone Model

Figure 11 a) and b) illustrate the experimental results compared to the 30 degree backbone model for the E-W and N-S directions respectively. Comparisons to the 30 degree backbone are made as the first four excursions to maximum in each direction occur during the 'leaves' of the protocol and cyclic degradation makes it unlikely that the uni-directional capacity will be reached in the later cycles. Shear failure occurred in the first 'leaf' of the 1.5% cycles as illustrated in Figure 10 a) above. At this point the displacement in the E-W direction was moderately less than the modelled shear failure displacement of 21.6 mm. Post shear failure the stiffness in the N-S direction is negative, and essentially is zero in the E-W direction. Axial failure then occurred on the subsequent 'leaf' after minimal additional displacement demand.

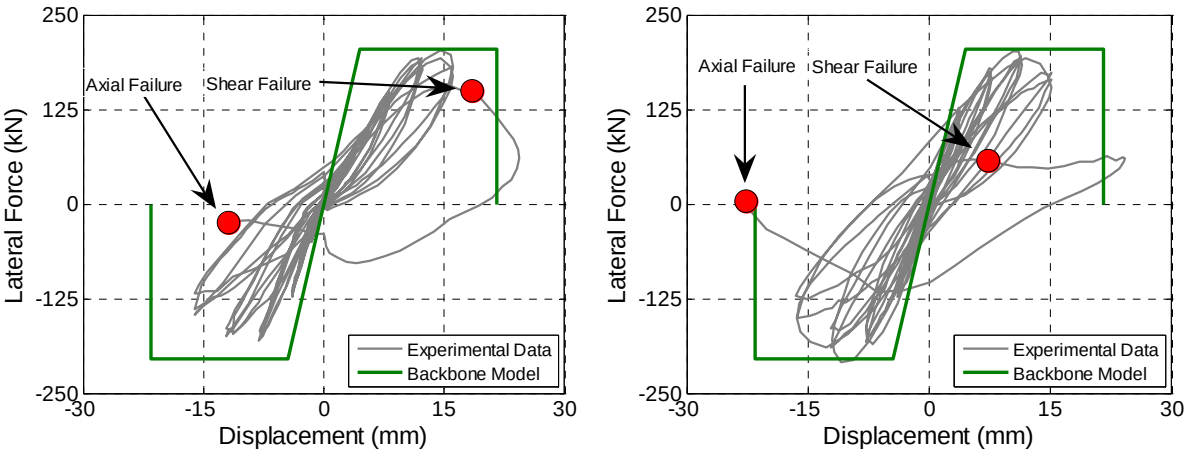

a) Model Comparison (E-W) **b) Model Comparison (N-S)**

Figure 11 Backbone Model and Experimental Comparison for Specimen 24L-300-3D

4 CONCLUSIONS

There are a number of conclusions available from testing to date: 1) it is evident that inadequately detailed RC gravity columns are extremely susceptible to loss of axial load carrying capacity at drift levels lower than expected during a design level seismic event. 2) bi-directional loading results in a significant reduction in the displacement capacity when compared to uni-directional loading. 3) the backbone model proposed by Elwood and Moehle (2006) is confirmed to adequately capture the shear and axial failure displacement limits of poorly detailed RC columns. 4) buckling of the cranked bars (initiating the shear failure plane of these cantilever tests) will not be a critical mechanism when full double curvature columns are considered.

Completion of the proposed experimental program is expected to further strengthen the conclusions to date. Further outcomes include: 1) an appropriate hysteresis rule for use in Inelastic Time-History Analysis can be identified and detail dependent calibration recommendations made. 2) limits corresponding to the splice plane failure of the cover concrete adjacent to the longitudinal bars can be determined. 3) recommendations regarding retrofit solutions to ensure adequate displacement capacity of these inadequately detailed RC columns be made.

REFERENCES:

Elwood, K., and Moehle, J. P. (2005a). "Drift Capacity of Reinforced Concrete Columns with Light Transverse Reinforcement." *Earthquake Spectra*, 21(1), 71-89.

Elwood, K. J., and Moehle, J. P. (2005b). "Axial Capacity Model for Shear-Damaged Columns." *ACI Structural Journal*, 102(4), 578-587.

Elwood, K. J., and Moehle, J. P. (2006). "Idealised Backbone Model For Existing Reinforced Concrete Columns and Comparisons With FEMA 356 Criteria." *Struct. Design Tall Spec. Build.*, 15, 553-569.

Lynn, A. C., Moehle, J. P., Mahin, S. A., and Holmes, W. T. (1996). "Seismic Evaluation of Existing Reinforced Concrete Building Columns." *Earthquake Spectra*, 12(4), 715-739.

Melek, M., Wallace, J. W., and Conte, J. P. (2003). "Experimental Assessment of Columns with Short Lap Splices Subjected to Cyclic Loads." *PEER Report*, 04.